JOURNAL OF THEORETICAL AND APPLIED MECHANICS
61, 1, pp. 175-187, Warsaw 2023
https://doi.org/10.15632/jtam-pl/158574

ON THE YIELD SURFACE OF A TYPICAL BENDING-DOMINANT PERIODIC LATTICE METAMATERIAL

Yongjun Wang, Jinxing Liu

Faculty of Civil Engineering and Mechanics, Jiangsu University, Zhenjiang, China

Corresponding author Jinxing Liu, e-mail: jxliu@mails.ucas.ac.cn

A theoretical method for analyzing the initial yield of a typical bending-dominant periodic lattice (BDPL) is established. Based on the principle of strain energy equivalence, the macroscopic effective stiffnesses of lattices are calculated. An empirical formula is employed to consider the contributions of both the axial force and bending moment. The initial yield surface of BDPL can be figured out by comparing the effective stress of each strut to the yield strength of the matrix material. The method is applicable to various BDPLs, which we believe is a helpful extension to the method for lattices comprising axial-tension bars in the literature.

Keywords: bending-dominant periodic lattice (BDPL), yield, metamaterial, strain energy equivalence

1. Introduction

With recent developments of additive manufacturing technologies, lattice metamaterials have been attracting more and more attentions from both industry and academia. It is a promising option in designs of metamaterials to choose lattice-type microstructures. Lattice materials can be divided into two types: stretching-dominant lattice and bending-dominant lattice (Deshpande *et al.*, 2001). Stretching-dominant lattices are famous for lightweight, high specific strength and stiffness (Evans *et al.*, 2001; Evans, 2001) and have been applied in many areas. Unlike stretching--dominant lattices, the bending-dominant lattices are used to provide other extraordinary mechanical properties such as negative Poisson's ratio (Chen *et al.*, 2017), compression-induced twist (Frenzel *et al.*, 2017), negative effective swelling (Liu *et al.*, 2016) and so on.

The macroscopic effective yield strength of lattice materials is an important index to evaluate its mechanical performance. It is also considered that yield behavior is a failure precursor of lattice materials and it plays a significant role in engineering designs. Thus, a comprehensive understanding on the yield behavior is of great necessity. An analytical initial yield surface equation of the octet-truss lattice material, which is a typical stretching-dominant lattice, was established by Deshpande *et al.* (2001). Wang and McDowell (2004, 2005) made a detailed theoretical derivation of six kinds of two-dimensional beam lattice structures and gave corresponding initial yield surfaces under both biaxial and triaxial stresses. Yield behavior of a range of honeycombs under uniaxial loads have also been investigated so far (Gibson, 2003; Wang and McDowell, 2005). Xue *et al.* (2005) proposed a phenomenological elliptic yield surface criterion based on the yield strength of stressing in different directions. Fan and Yang (2006) deduced three-dimensional yield surfaces of several stretching-dominant lattice materials.

To date, unlike stretching-dominant lattices, yield properties of BDPLs have been rarely reported. It can be imagined that BDPLs can have a very different yield response when compared with the stretching-dominant lattices because of the coupling of axial deformation and bending

deformation. This is our present focus. We assume that the in-plane (xy plane) deformation can be taken as a plane strain problem.

This paper is structured as follows. In Section 2, a new method used to investigate the yield behavior of BDPL is briefly presented. In Section 3, based on the principle of strain energy equivalence (PSEE) and finite element simulation, we obtain the constitutive equation of BDPL. The geometry equation is derived in Section 4. In Section 5, the stiffness matrix of a unit cell is calculated. The initial yield surfaces of BDPL are obtained in Section 6. The paper ends with conclusions in Section 7.

2. Material and methods

2.1. Material

The schematic diagram of BDPL is shown in Fig. 1a. Based on the previous work (Wang *et al.*, 2020), we adopt a specimen with an enough number of cells to reduce the influence of boundary conditions. Geometric parameters T, H and W the thickness, height and width of BDPL, respectively. The unit cell is shown in Fig. 1b, which is composed of four curved bars with the same curvature radius r and central angle α. For each strut, its thickness is b and the spacing between two ends is L. The dimensions of BDPL are as follows: $H = W = 100\,\text{mm}$, $T = 10\,\text{mm}$, $b = 1\,\text{mm}$, $L = 4.762\,\text{mm}$ and the central angle $\alpha = 60°$. The adopted matrix material is Aluminum, with density $\rho = 2700\,\text{kg/m}^3$, Young's modulus E and Poisson's ratio ν 70 GPa and 0.33, respectively, and yield strength $\sigma_Y = 110\,\text{MPa}$.

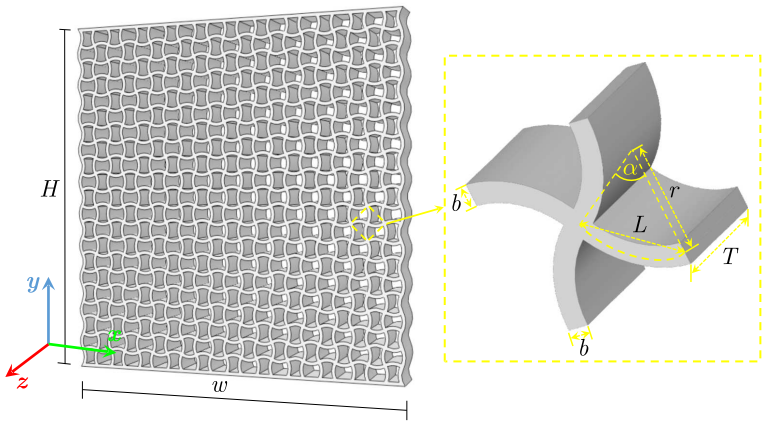

Fig. 1. Schematic of the lattice: (a) the whole structure and (b) the unit cell

2.2. Methods

The present research roadmap is shown in Fig. 2. Based on the principle of strain energy equivalence, the macroscopic effective stiffnesses of the lattice are calculated. The relation between the displacements of lattice joints and the macroscopic uniform strain prescribed can be obtained by combining a method of particular displacement fields (MPDF) and finite element analyses. Furthermore, by analyzing the relation between deformation and stress of a single periodic unit cell, forces on both ends of each curved strut can be expressed as a linear function of the macroscopic stresses. An empirical formula for calculating the effective stress is employed to consider the contributions of both the axial force and bending moment. Finally, the initial yield surface of BDPL can be figured out by comparing the effective stress of each curved strut to the yield strength of the matrix material.

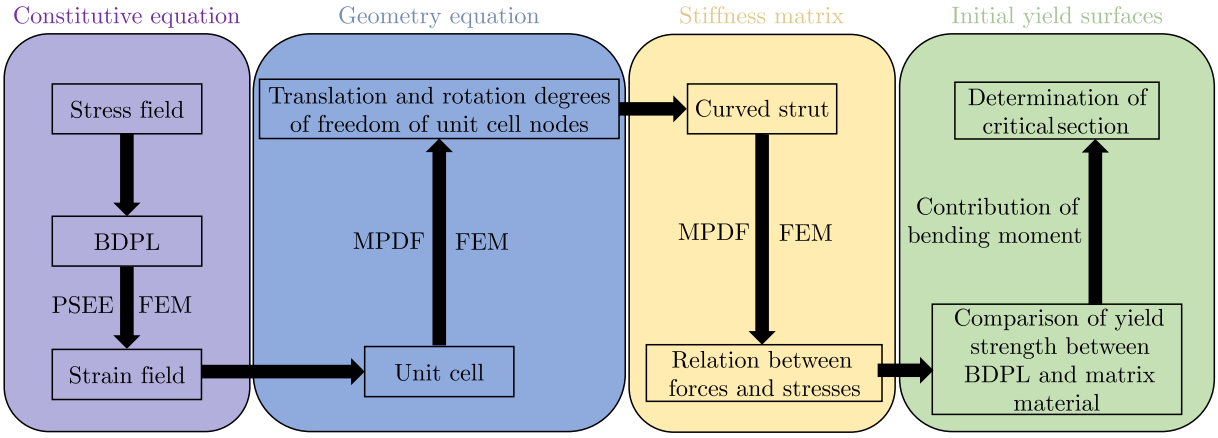

Fig. 2. The present research roadmap

3. Constitutive equation

A representative unit cell is used to replace BDPL, as shown in Fig. 3. The effective modulus of elasticity of BDPL is calculated by using an equivalent uniform medium with the same effective mechanical properties. This equivalence is established by equalizing the strain energies of two media (discrete and continuous) under the same loading and boundary conditions. Usually, a uniform strain field is prescribed for simplicity. According to the principle of strain energy equivalence, we have

$$U_{discrete} = U_{continuum} \tag{3.1}$$

The strain energy of the discrete unit cell is expressed as

$$U_{discrete} = \sum_{i=1}^{n} U^i \tag{3.2}$$

where U^i represents the energy stored in the i-th curved strut, n stands for the total number of struts in a single unit cell. The strain energy of the equivalent continuum is written as

$$U_{continuum} = \frac{1}{2} \int_V \sigma\varepsilon \, dV \tag{3.3}$$

It is notable that in Eq. (3.3), $V = At$ under the assumed plane strain condition, and the integral over V is actually over A. This meaning for volume V remains unchanged throughout this article.

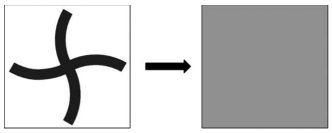

Fig. 3. Geometry of discrete and continuum unit cells

Under the plane stress conditions, the continuum constitutive equation is given in terms of the effective stiffness matrix C_{ij} by

$$\begin{Bmatrix} \sigma_{11} \\ \sigma_{22} \\ \sigma_{12} \end{Bmatrix} = \begin{bmatrix} C_{11} & C_{12} & 0 \\ C_{21} & C_{22} & 0 \\ 0 & 0 & C_{66} \end{bmatrix} \begin{Bmatrix} \varepsilon_{11} \\ \varepsilon_{22} \\ \varepsilon_{12} \end{Bmatrix} \tag{3.4}$$

where the elastic constants C_{11}, C_{22}, C_{12} and C_{21} in the matrix are calculated by finite element simulations one by one by prescribing proper uniform strain ε_{ij} fields. The designated displacements on the boundaries are given by

$$u_i = \varepsilon_{ij} X_j \qquad i,j = 1,2 \tag{3.5}$$

and X_i represents the coordinate of the boundary. Considering $C_{12} = C_{21}$, the strain energy of continuum is written as

$$U = \frac{V}{2}\sigma_{ij}\varepsilon_{ij} = [C_{11}(\varepsilon_{11})^2 + C_{22}(\varepsilon_{22})^2 + C_{66}(\varepsilon_{12})^2 + 2C_{12}(\varepsilon_{11})(\varepsilon_{22})] \tag{3.6}$$

Equation (3.6) can be numerically determined once the corresponding strain energy is obtained from finite element examples. For example, under the loading conditions shown in Fig. 4a, namely ε_{11} is specified and $\varepsilon_{22}, \varepsilon_{12} = 0$, the strain energy can be expressed as

$$U = \frac{V}{2}C_{11}(\varepsilon_{11})^2 \tag{3.7}$$

from which, the elastic constant C_{11} can be obtained. Similarly, the other elastic constants C_{22}, C_{12} and C_{66} can also be obtained by various specific finite element examples:
— for C_{22}: $\varepsilon_{11} = \varepsilon_{12} = 0$, $\varepsilon_{22} =$ const

$$U = \frac{V}{2}C_{22}(\varepsilon_{22})^2 \tag{3.8}$$

— for C_{12}: $\varepsilon_{11} =$ const , $\varepsilon_{12} = 0$, $\varepsilon_{22} =$ const

$$U = \frac{V}{2}[C_{11}(\varepsilon_{11})^2 + C_{22}(\varepsilon_{22})^2 + 2C_{12}(\varepsilon_{11})(\varepsilon_{22})] \tag{3.9}$$

— for C_{66}: $\varepsilon_{11} = \varepsilon_{22} = 0$, $\varepsilon_{12} =$ const

$$U = \frac{V}{2}C_{66}(\varepsilon_{12})^2 \tag{3.10}$$

Once the values of C_{11}, C_{22}, C_{12} and C_{66} are obtained, Young's modulus and Poisson's ratio of BDPL can be given as

$$\begin{aligned} E_1 &= \frac{C_{11}C_{22} - C_{12}^2}{C_{22}} \qquad E_2 = \frac{C_{11}C_{22} - C_{21}^2}{C_{11}} \\ \nu_{12} &= \frac{C_{12}}{C_{22}} \qquad \nu_{21} = \frac{C_{21}}{C_{11}} \end{aligned} \tag{3.11}$$

The finite element software Abaqus is used to simulate the response of lattice plates under above various boundary conditions. The BDPL plate has 21 curved struts along horizontal and vertical directions respectively. Element B21 with a mesh sweeping seed size of 0.1 mm was employed for simulations. Each strut between joints is divided into 10 beam elements to ensure the accuracy of simulation results, which is confirmed by comparing with the results under finer 15 elements per strut (error less than 1%). The parameter setting mentioned in Section 2.1 is employed. In the following, we list out the boundary conditions for calculating the effective moduli.

For calculating C_{11} (Fig. 4a and Eq. (3.7))

$$\begin{aligned} &u(0,y,z) = v(0,y,z) = 0 \qquad v(x,0,z) = v(x,H,z) = 0 \\ &u(W,y,z) = \text{ const} \qquad w(x,y,0) = w(x,y,T) = 0 \end{aligned} \tag{3.12}$$

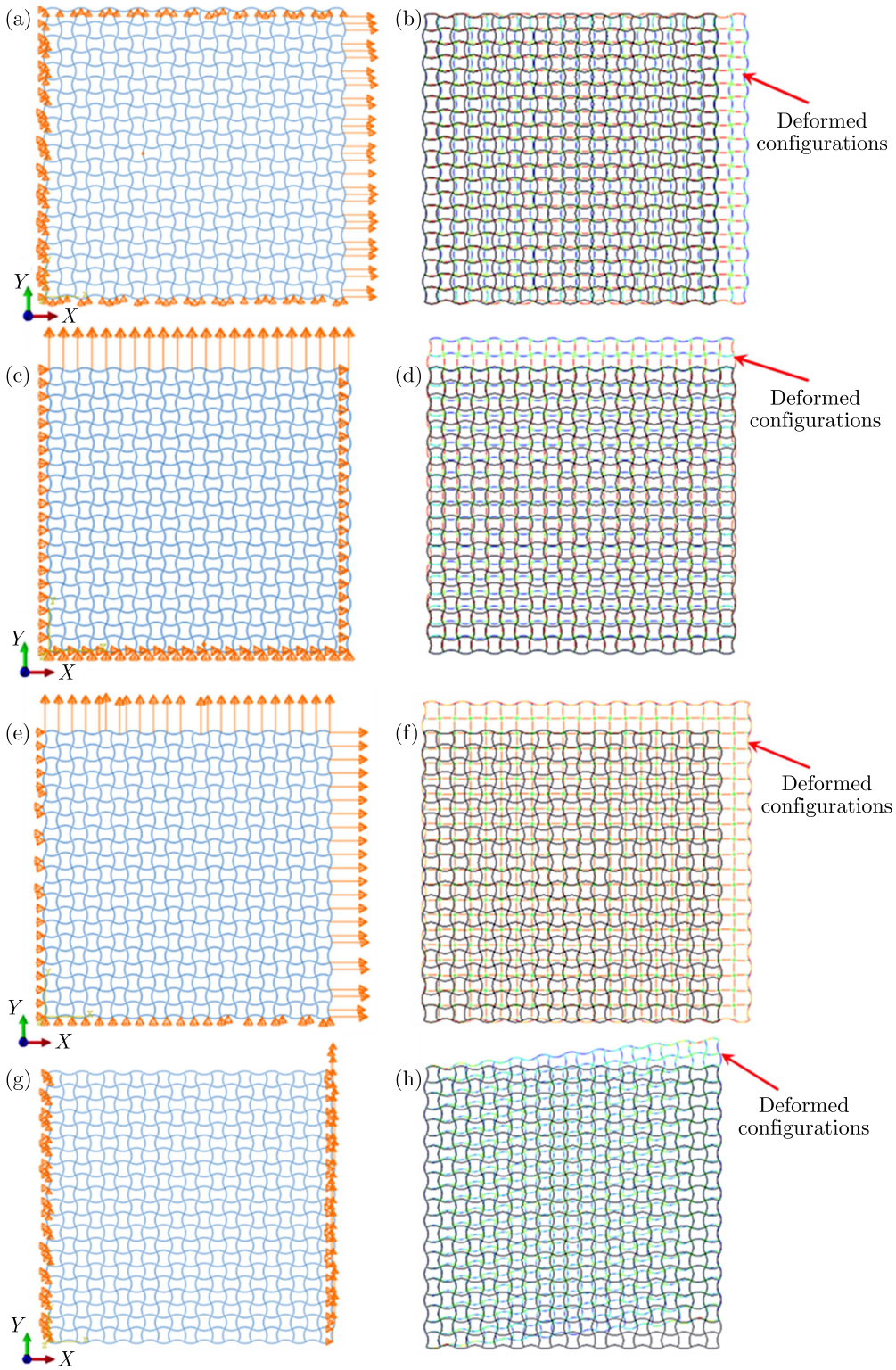

Fig. 4. (a), (c), (e) and (g) – Loading and boundary conditions for calculating C_{11}, C_{22}, C_{12} and C_{66}, respectively; (b), (d), (f), (h) – comparison between undeformed and deformed configurations

where, under the plane strain condition, three displacement components are functions of x and y, and are irrelated to z, i.e. $u(x, y, z) = u(x, y)$. The formula including z is simple for explicit prescribing the boundary conditions in FEM simulations.

For calculating C_{22} (Fig. 4c and Eq. (3.8))

$$\begin{aligned} &u(0,x,y,z) = u(W,y,z) = 0 \qquad u(x,0,z) = v(x,0,z) = 0 \\ &v(x,H,z) = \text{ const} \qquad w(x,y,0) = w(x,y,T) = 0 \end{aligned} \tag{3.13}$$

For calculating C_{12} (Fig. 4e and Eq. (3.9))

$$\begin{aligned} &u(0,y,z) = 0 \qquad v(x,0,z) = 0 \\ &u(W,y,z) = v(x,H,z) = \text{ const} \qquad w(x,y,0) = w(x,y,T) = 0 \end{aligned} \tag{3.14}$$

For calculating C_{66} (Fig. 4g and Eq. (3.10)

$$\begin{aligned} &u(0,y,z) = v(0,x,y,z) = 0 \qquad v(x,W,z) = \text{ const} \\ &u(x,W,z) = 0 \qquad w(x,y,0) = w(x,y,T) = 0 \end{aligned} \tag{3.15}$$

where u, v and w represent the displacements along the x, y and z direction, respectively.

Young's modulus and Poisson's ratio of BDPL in the x and y direction are obtained from Eq. (3.11)

$$E_1 = E_2 = 6.50\,\text{GPa} \qquad \nu_{12} = \nu_{21} = -0.32 \tag{3.16}$$

It can be seen that the studied BDPL has a negative Poisson's ratio.

The continuum constitutive equation under the plane stress condition is expressed by the stiffness matrix

$$\begin{Bmatrix} \sigma_{11} \\ \sigma_{22} \\ \sigma_{12} \end{Bmatrix} = \underbrace{\begin{bmatrix} C_{11} & C_{12} & 0 \\ C_{21} & C_{22} & 0 \\ 0 & 0 & C_{66} \end{bmatrix}}_{\text{Effective stiffness matrix}} \begin{Bmatrix} \varepsilon_{11} \\ \varepsilon_{22} \\ \varepsilon_{12} \end{Bmatrix} = 10^9 \begin{bmatrix} 7.24 & -2.31 & 0 \\ -2.31 & 7.24 & 0 \\ 0 & 0 & 1.00 \end{bmatrix} \begin{Bmatrix} \varepsilon_{11} \\ \varepsilon_{22} \\ \varepsilon_{12} \end{Bmatrix} \tag{3.17}$$

Then the compliance matrix $\mathbf{S}$ can be obtained by inverting the effective stiffness matrix shown in equation (3.17), i.e.

$$\begin{Bmatrix} \varepsilon_{11} \\ \varepsilon_{22} \\ \varepsilon_{12} \end{Bmatrix} = \underbrace{10^{-10} \begin{bmatrix} 1.54 & 0.49 & 0 \\ 0.49 & 1.54 & 0 \\ 0 & 0 & 10.00 \end{bmatrix}}_{\mathbf{S}} \begin{Bmatrix} \sigma_{11} \\ \sigma_{22} \\ \sigma_{12} \end{Bmatrix} \tag{3.18}$$

4. Geometry equation

The relation between the displacements of lattice joints and the macroscopic uniform strain prescribed can be obtained by combining the method of particular displacement fields and finite element analyses. As shown in Fig. 5, a unit cell comprises five joints and each joint has translational and rotational degrees of freedom. Symbols u_i, v_i and φ_i, represent horizontal, vertical displacement and rotation angle, respectively, and the subscript i is the joint number.

The specified uniform strain fields on the BDPL shown in Fig. 4a are $\varepsilon_{11} = 10^{-3}$, and $\varepsilon_{11} = \varepsilon_{22} = 0$. The displacements and rotation angle of each unit cell joint are extracted, as shown in the second column of Appendix A. Similarly, under the uniform strain fields like $\varepsilon_{22} = 10^{-3}$, $\varepsilon_{11} = \varepsilon_{12} = 0$ (Fig. 4c) and $\varepsilon_{12} = 5 \cdot 10^{-4}$, $\varepsilon_{11} = \varepsilon_{22} = 0$ (Fig. 4g), the displacements and rotation angle of each unit cell joint are also obtained in Appendix A. The relation between displacements of each joint in the unit cell and different macroscopic uniform strain fields can be derived from Appendix A. The geometry equation is simply written as

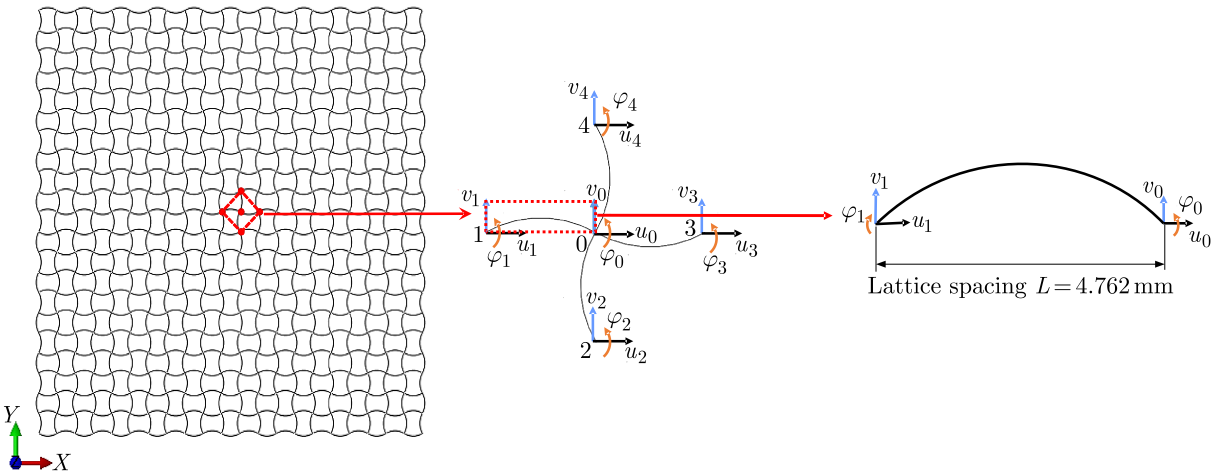

Fig. 5. (a) Schematic of the studied BDPL, (b) translational and rotational degrees of freedom and (c) the curved beam composing the unit cell

$$\left\{u_0 \quad v_0 \quad \varphi_0 \quad \cdots \quad u_4 \quad v_4 \quad \varphi_4\right\}^{\mathrm{T}} = \mathbf{B}_{15\times 3}\left\{\varepsilon_{11} \quad \varepsilon_{22} \quad \varepsilon_{12}\right\}^{\mathrm{T}} \tag{4.1}$$

The specific equation is found as given in Appendix B.

5. Stiffness matrix of unit cell

In order to obtain the stiffness matrix of a unit cell, it is needed to investigate the stiffness matrix of each curved strut in the unit cell firstly. We continue to use the method of particular displacement fields. We take out a curved strut from the unit cell, fix five degrees of freedom and give a prescribed value to the remaining one. The forces and bending moments of endpoints can be obtained from Abaqus. In this Section, the prescribed displacement and rotation angle are 10^{-4} mm and 10^{-4} rad, respectively.

Taking 1-0 strut as an example, the stiffness matrix of a single curved strut is obtained as

$$\begin{Bmatrix} F_{x_1} \\ F_{y_1} \\ M_1 \\ F_{x0}^{(1-0)} \\ F_{y0}^{(1-0)} \\ M_0^{(1-0)} \end{Bmatrix} = \mathbf{A}^{(1-0)} \begin{Bmatrix} u_1 \\ v_1 \\ \varphi_1 \\ u_0 \\ v_0 \\ \varphi_0 \end{Bmatrix} \tag{5.1}$$

The calculated parameters of $\mathbf{A}^{(1-0)}$ are given in Appendix B.

The incidence matrices in Eqs. (4.1) and (3.18) are denoted as $\mathbf{B}$ and $\mathbf{S}$, respectively. The displacement and strain incidence matrix $\mathbf{B}^{(1-0)}$ for the joint pair comprising 0 and 1 can be extracted from $\mathbf{B}$. Finally, the forces on both ends of each curved strut can be expressed as a linear function of the macroscopic stresses

$$\begin{Bmatrix} F_{x_i} \\ F_{y_i} \\ M_i \\ F_{x0}^{(i-0)} \\ F_{y0}^{(i-0)} \\ M_0^{(i-0)} \end{Bmatrix} = \mathbf{A}^{(i-0)}\mathbf{B}^{(i-0)}\mathbf{S} \begin{Bmatrix} \sigma_{11} \\ \sigma_{22} \\ \sigma_{12} \end{Bmatrix} \qquad i = 1,2,3,4 \tag{5.2}$$

6. Initial yield surfaces of BDPL

6.1. Empirical formula

An empirical formula (Liu *et al.*, 2008) for calculating the effective stress is employed to consider the contributions of both the axial force and bending moment. The effective stress in the curved strut is defined as

$$\sigma = \frac{N}{A} + a\frac{(|M_i|, |M_j|)_{max}}{W_z} \tag{6.1}$$

As shown in Fig. 6, where N is the normal force in the considered strut, M_i and M_j are the bending moments at the joint i and j of the strut, W_z is the section modulus. The coefficient a plays a role in regulating the contribution of the bending moment to the effective stress. Lilliu and van Mier (2003) set the coefficient to 0.005 (Karihaloo *et al.*, 2003; Liu *et al.*, 2007). In order to investigate the effects of this parameter, a is set to 0.005 and 0.0075.

For a particular stress status, it is necessary to find out the curved strut easiest to yield among the unit cells subjected to the prescribed macroscopic strain field.

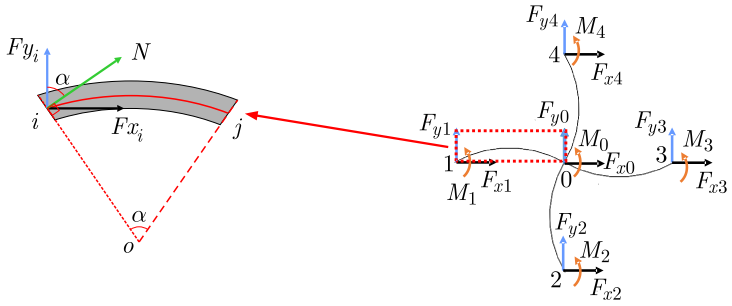

Fig. 6. (a) Curved strut, (b) schematic of end forces and moments of the unit cell

6.2. Yield surface calculations

According to the geometric parameters in Section 2.1, the section area A of the strut and section modulus W_z are $10^{-5}\,\mathrm{m}^2$, $(1/6)\cdot 10^{-3}\,\mathrm{m}^3$, respectively. The linear function between the effective stresses and forces in $(\varepsilon_{11}, \varepsilon_{22})$ space is easily obtained from Eq. (5.2).

For 1-0 strut, we have

$$N = F_{x_1}\cos 30^\circ + F_{y_1}\sin 30^\circ \tag{6.2}$$

From equation (6.1), the effective stress can be expressed in the form

$$|\sigma| = \left|\left(\frac{N}{A}\right)_{max}\right| + \left|a\frac{M_0}{W_z}\right|_{max} = |(-4.77\sigma_{11} + 0.36\sigma_{22})_{max}| + |(600aM_0)_{max}| \tag{6.3}$$

where, the operation of simply considering the maximum effective normal stress indicates that the source material has been assumed as isotropic.

The value of a is set to 0.005, the effective stress can be calculated as

$$|\sigma| = \left|\left(\frac{N}{A}\right)_{max}\right| + \left|\alpha\frac{M_0}{W_z}\right|_{max} = \begin{cases} 7.05\sigma_{11} + 2.73\sigma_{22} & \text{for} \quad \sigma_{11} > 0, \quad \sigma_{22} > 0 \\ 7.05\sigma_{11} - 2.73\sigma_{22} & \text{for} \quad \sigma_{11} > 0 \quad \sigma_{22} < 0 \\ -7.05\sigma_{11} + 2.73\sigma_{22} & \text{for} \quad \sigma_{11} < 0 \quad \sigma_{22} > 0 \\ -7.05\sigma_{11} - 2.73\sigma_{22} & \text{for} \quad \sigma_{11} < 0 \quad \sigma_{22} < 0 \end{cases} \tag{6.4}$$

the yield surface of 1-0 strut is given by

$$\frac{\sigma_{22}}{\sigma_Y}=\begin{cases} -2.58\dfrac{\sigma_{11}}{\sigma_Y}+0.37 & \text{for} \quad \sigma_{11}>0 \quad \sigma_{22}>0 \\ 2.58\dfrac{\sigma_{11}}{\sigma_Y}-0.37 & \text{for} \quad \sigma_{11}>0 \quad \sigma_{22}<0 \\ 2.58\dfrac{\sigma_{11}}{\sigma_Y}+0.37 & \text{for} \quad \sigma_{11}<0 \quad \sigma_{22}>0 \\ -2.58\dfrac{\sigma_{11}}{\sigma_Y}-0.37 & \text{for} \quad \sigma_{11}<0 \quad \sigma_{22}<0 \end{cases} \tag{6.5}$$

where σ_Y is the yield stress of the matrix material.

Similarly, for curved struts 2-0, 3-0 and 4-0, the yield surfaces are calculated as follows:

— 2-0

$$\frac{\sigma_{22}}{\sigma_Y}=\begin{cases} -0.39\dfrac{\sigma_{11}}{\sigma_Y}+0.14 & \text{for} \quad \sigma_{11}>0 \quad \sigma_{22}>0 \\ 0.39\dfrac{\sigma_{11}}{\sigma_Y}-0.14 & \text{for} \quad \sigma_{11}>0 \quad \sigma_{22}<0 \\ 0.39\dfrac{\sigma_{11}}{\sigma_Y}+0.14 & \text{for} \quad \sigma_{11}<0 \quad \sigma_{22}>0 \\ 0.39\dfrac{\sigma_{11}}{\sigma_Y}-0.14 & \text{for} \quad \sigma_{11}<0 \quad \sigma_{22}<0 \end{cases} \tag{6.6}$$

— 3-0

$$\frac{\sigma_{22}}{\sigma_Y}=\begin{cases} -2.58\dfrac{\sigma_{11}}{\sigma_Y}+0.37 & \text{for} \quad \sigma_{11}>0 \quad \sigma_{22}>0 \\ 2.58\dfrac{\sigma_{11}}{\sigma_Y}-0.37 & \text{for} \quad \sigma_{11}>0 \quad \sigma_{22}<0 \\ 2.58\dfrac{\sigma_{11}}{\sigma_Y}+0.37 & \text{for} \quad \sigma_{11}<0 \quad \sigma_{22}>0 \\ -2.58\dfrac{\sigma_{11}}{\sigma_Y}-0.37 & \text{for} \quad \sigma_{11}<0 \quad \sigma_{22}<0 \end{cases} \tag{6.7}$$

— 4-0:

$$\frac{\sigma_{22}}{\sigma_Y}=\begin{cases} -0.39\dfrac{\sigma_{11}}{\sigma_Y}+0.14 & \text{for} \quad \sigma_{11}>0 \quad \sigma_{22}>0 \\ 0.39\dfrac{\sigma_{11}}{\sigma_Y}-0.14 & \text{for} \quad \sigma_{11}>0 \quad \sigma_{22}<0 \\ 0.39\dfrac{\sigma_{11}}{\sigma_Y}+0.14 & \text{for} \quad \sigma_{11}<0 \quad \sigma_{22}>0 \\ -0.39\dfrac{\sigma_{11}}{\sigma_Y}-0.14 & \text{for} \quad \sigma_{11}<0 \quad \sigma_{22}<0 \end{cases} \tag{6.8}$$

From equations (6.5) to (6.8), we find that strut 1-0 has the same yield surface with strut 3-0, while strut 2-0 has the same yield surface with strut 4-0. The initial yield surface of BDPL in $(\sigma_{11}, \sigma_{22})$ space is sketched in Fig. 7. The region beyond dashed lines represents the yield of each strut in the stress space. It can be considered that the area within the red solid lines keeps elastic without any strut yielding. In Fig. 8, the influence of parameter a is discussed. With an increase of a, the area surrounded by the yield surface decreases. The straight struts lattice can be considered as a special curved strut lattice with the central angle $\alpha = 0°$. In Fig. 9, the yield surface of the straight struts lattice is calculated, and it can be seen that the tensile and compressive strength of the straight struts lattice is better than the curved struts lattice.

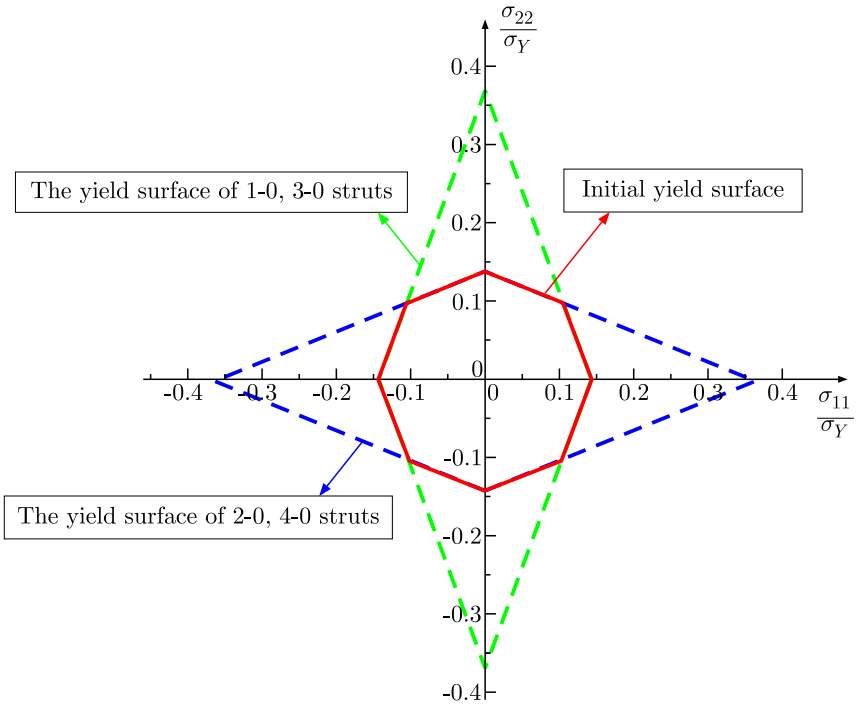

Fig. 7. The initial yield surface in $(\sigma_{11}, \sigma_{22})$ space of unit cell of BDPL

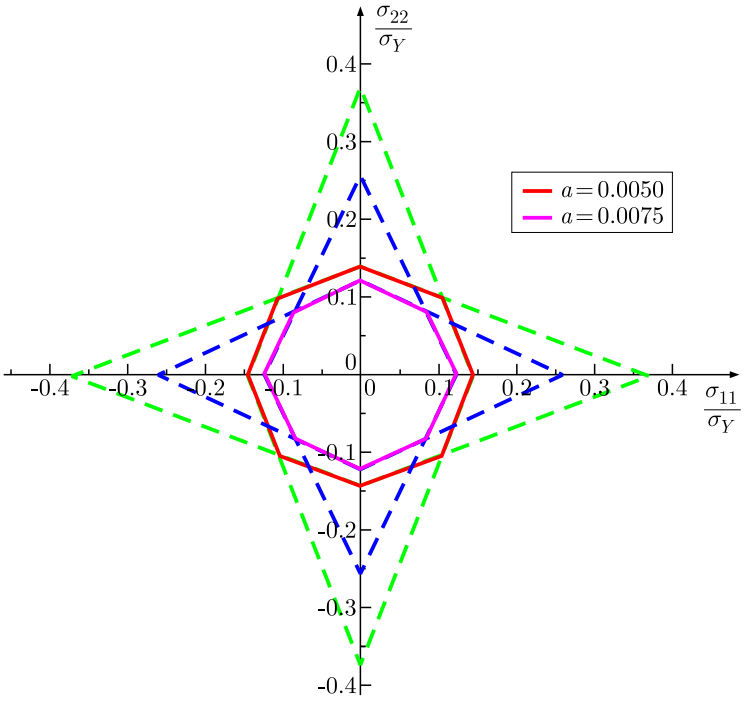

Fig. 8. The influence of a on initial yield surfaces of the unit cell of BDPL in $(\sigma_{11}, \sigma_{22})$ space

7. Conclusions

In this study, based on the principle of strain energy equivalence, the macroscopic effective stiffnesses of the corresponding equivalent continuum are calculated. The relation between the displacements of lattice joints and the macroscopic uniform strain prescribed have been obtained by combining the particular-displacement method and finite element analyses. By analyzing the

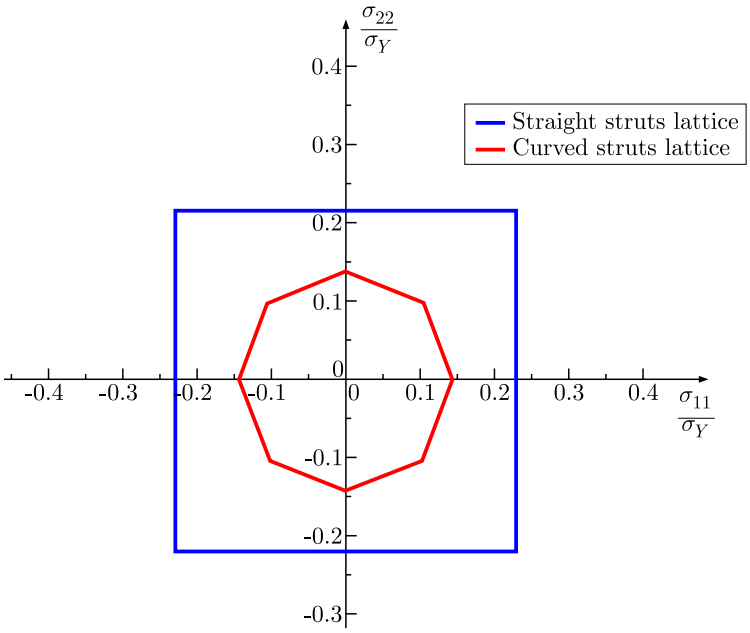

Fig. 9. The initial yield surface of the straight struts lattice ($\alpha = 0°$) and the curved struts lattice ($\alpha = 60°$) in $(\sigma_{11}, \sigma_{22})$ space

relation between deformation and stress of a single periodic unit cell, the forces on both ends of each curved strut can be expressed as a linear function of the macroscopic stresses. The yield surfaces are calculated successfully. Compared with the existing methods in the literature, the proposed method is convenient to deal with the yield problem of bending-dominant lattice metamaterials such as the curved strut lattice.

Particularly, an empirical formula for calculating the effective stress has been employed to consider the contributions of both the axial force and bending moment, by introducing a parameter a adjusting the relative contribution of bending to yield strength. It is found that a larger value of a leads to a lower yield strength.

Acknowledgements

The work was supported by the National Science Foundation of China (Grant No. 11972174 and Grant No. 11672119).

Appendix A

Table 1. Displacements and rotation angle of each unit cell joint

Displacement [mm] Rotation angle [rad]	Uniform strain fields		
	$\varepsilon_{11} = 10^{-3}$, $\varepsilon_{22} = \varepsilon_{12} = 0$	$\varepsilon_{22} = 10^{-3}$, $\varepsilon_{11} = \varepsilon_{12} = 0$	$\varepsilon_{12} = 5 \cdot 10^{-4}$, $\varepsilon_{11} = \varepsilon_{22} = 0$
u_0	$4.76 \cdot 10^{-2}$	$-3.39 \cdot 10^{-5}$	$7.42 \cdot 10^{-6}$
v_0	$-3.38 \cdot 10^{-5}$	$4.76 \cdot 10^{-2}$	$4.75 \cdot 10^{-2}$
φ_0	$1.65 \cdot 10^{-3}$	$1.65 \cdot 10^{-3}$	$5.33 \cdot 10^{-4}$
u_1	$4.28 \cdot 10^{-2}$	$-1.02 \cdot 10^{-4}$	$6.52 \cdot 10^{-6}$
v_1	$-3.38 \cdot 10^{-5}$	$4.76 \cdot 10^{-2}$	$4.24 \cdot 10^{-2}$

φ_1	$-1.65 \cdot 10^{-3}$	$-1.65 \cdot 10^{-3}$	$5.31 \cdot 10^{-4}$
u_2	$4.76 \cdot 10^{-2}$	$-3.38 \cdot 10^{-5}$	$2.59 \cdot 10^{-5}$
v_2	$-1.02 \cdot 10^{-4}$	$4.28 \cdot 10^{-2}$	$4.75 \cdot 10^{-2}$
φ_2	$-1.65 \cdot 10^{-3}$	$-1.65 \cdot 10^{-3}$	$5.33 \cdot 10^{-4}$
u_3	$5.24 \cdot 10^{-2}$	$3.38 \cdot 10^{-5}$	$7.42 \cdot 10^{-6}$
v_3	$-3.38 \cdot 10^{-4}$	$4.76 \cdot 10^{-2}$	$5.25 \cdot 10^{-2}$
φ_3	$-1.65 \cdot 10^{-3}$	$-1.65 \cdot 10^{-3}$	$5.33 \cdot 10^{-4}$
u_4	$4.76 \cdot 10^{-2}$	$-3.38 \cdot 10^{-5}$	$-7.42 \cdot 10^{-6}$
v_4	$3.38 \cdot 10^{-5}$	$5.24 \cdot 10^{-2}$	$4.75 \cdot 10^{-2}$
φ_4	$-1.65 \cdot 10^{-3}$	$-1.65 \cdot 10^{-3}$	$5.33 \cdot 10^{-4}$

Appendix B

The specific parameters of the matrices mentioned in the article are as follows

$$\mathbf{A}^{(1-0)} = 10^6 \begin{bmatrix} 1.19 \cdot 10^2 & 0 & -4.99 \cdot 10^{-2} & -1.19 \cdot 10^2 & 0 & 4.99 \cdot 10^{-2} \\ & 4.51 \cdot 10^1 & 1.07 \cdot 10^{-1} & 0 & -4.51 \cdot 10^1 & 1.07 \cdot 10^{-1} \\ & & 1.45 \cdot 10^{-3} & 4.99 \cdot 10^{-2} & -1.07 \cdot 10^{-1} & -9.36 \cdot 10^{-4} \\ & \text{Sym} & & 1.19 \cdot 10^2 & 0 & -4.99 \cdot 10^{-2} \\ & & & & 4.51 \cdot 10^1 & -1.07 \cdot 10^{-1} \\ & & & & & 1.45 \cdot 10^{-3} \end{bmatrix} \tag{B.1}$$

$$\begin{Bmatrix} u_0 \\ v_0 \\ \varphi_0 \\ u_1 \\ v_1 \\ \varphi_1 \\ u_2 \\ v_2 \\ \varphi_2 \\ u_3 \\ v_3 \\ \varphi_3 \\ u_4 \\ v_4 \\ \varphi_4 \end{Bmatrix} = 10^{-6} \underbrace{\begin{bmatrix} 4.76 \cdot 10^4 & -3.38 \cdot 10^1 & 1.49 \cdot 10^1 \\ -3.38 \cdot 10^1 & 4.76 \cdot 10^4 & 9.49 \cdot 10^4 \\ 1.65 \cdot 10^6 & 1.65 \cdot 10^6 & 1.07 \cdot 10^6 \\ 4.28 \cdot 10^4 & -1.02 \cdot 10^2 & 1.30 \cdot 10^1 \\ -3.38 \cdot 10^1 & 4.76 \cdot 10^4 & 8.48 \cdot 10^4 \\ -1.65 \cdot 10^6 & -1.65 \cdot 10^6 & 1.06 \cdot 10^6 \\ 4.76 \cdot 10^4 & -3.38 \cdot 10^1 & 5.19 \cdot 10^1 \\ -1.02 \cdot 10^2 & 4.28 \cdot 10^4 & 9.49 \cdot 10^4 \\ -1.65 \cdot 10^6 & -1.65 \cdot 10^6 & 1.07 \cdot 10^6 \\ 5.24 \cdot 10^4 & 3.38 \cdot 10^1 & 1.49 \cdot 10^1 \\ -3.38 \cdot 10^1 & 4.76 \cdot 10^4 & 1.05 \cdot 10^5 \\ -1.65 \cdot 10^6 & -1.65 \cdot 10^6 & 1.07 \cdot 10^6 \\ 4.76 \cdot 10^4 & -3.38 \cdot 10^1 & -1.49 \cdot 10^1 \\ 3.38 \cdot 10^1 & 5.24 \cdot 10^4 & 9.49 \cdot 10^4 \\ -1.65 \cdot 10^6 & -1.65 \cdot 10^6 & 1.07 \cdot 10^6 \end{bmatrix}}_{\mathbf{B}_{(15\times 3)}} \begin{Bmatrix} \varepsilon_{11} \\ \varepsilon_{22} \\ \varepsilon_{12} \end{Bmatrix} \tag{B.2}$$

References

1. Chen Y., Li T., Scarpa F., Wang L., 2017, Lattice metamaterials with mechanically tunable Poisson's ratio for vibration control, *Physical Review Applied*, **7**, 024012
2. Deshpande V., Ashby M., Fleck N., 2001, Foam topology: bending versus stretching dominated architectures, *Acta Materialia*, **49**, 1035-1040

3. Deshpande V.S., Fleck N.A., Ashby M.F., 2001, Effective properties of the octet-truss lattice material, *Journal of the Mechanics and Physics of Solids*, **49**, 1747-1769

4. Evans A., 2001, Lightweight materials and structures, *MRS Bulletin*, **26**, 790-797

5. Evans A.G., Hutchinson J.W., Fleck N.A., Ashby M.F., Wadley H.N.G., 2001, The topological design of multifunctional cellular metals, *Progress in Materials Science*, **46**, 309-327

6. Fan H., Yang W., 2006, An equivalent continuum method of lattice structures, *Acta Mechanica Solida Sinica*, **19**, 103-113

7. Frenzel T., Kadic M., Wegener M., 2017, Three-dimensional mechanical metamaterials with a twist, *Science*, *358*, 1072-1074

8. Gibson L.J., 2003, Cellular solids, *MRS Bulletin*, **28**, 270-274

9. Karihaloo B.L., Shao P.F., Xiao Q.Z., 2003, Lattice modelling of the failure of particle composites, *Engineering Fracture Mechanics*, **70**, 2385-2406

10. Lilliu G., van Mier J.G., 2003, 3D lattice type fracture model for concrete, *Engineering Fracture Mechanics*, **70**, 927-941

11. Liu J., Gu T., Shan S., Sung H.K., Weaver J.C., Bertoldi K., 2016, Harnessing buckling to design architected materials that exhibit effective negative swelling, *Advanced Materials*, **28**, 6619-6624

12. Liu J.X., Deng S.C., Zhang J., Liang N.G., 2007, Lattice type of fracture model for concrete, *Theoretical and Applied Fracture Mechanics*, **48**, 269-284

13. Liu J.X., Zhao Z.Y., Deng S.C., Liang N.G., 2008, A simple method to simulate shrinkage-induced cracking in cement-based composites by lattice-type modeling, *Computational Mechanics*, **43**, 477-492

14. Wang A., McDowell D., 2004, The in-plane mechanical properties of various periodic honeycombs, *Journal of Engineering of Material and Technology*, **126**, 137-156

15. Wang A., McDowell D., 2005, Yield surfaces of various periodic metal honeycombs at intermediate relative density, *International Journal of Plasticity*, **21**, 285-320

16. Wang Y., Chi Z., Liu J., 2020, On buckling behaviors of a typical bending-dominated periodic lattice, *Composite Structures*, **258**, 113204

17. Xue Z., Vaziri A., Hutchinson J.W., 2005, Non-uniform hardening constitutive model for compressible orthotropic materials with application to sandwich plate cores, *Computer Modeling in Engineering and Sciences*, **10**, 79

Manuscript received July 27, 2022; accepted for print November 18, 2022